Journal of Zhejiang University-SCIENCE A (Applied Physics & Engineering)
ISSN 1673-565X (Print); ISSN 1862-1775 (Online)
www.jzus.zju.edu.cn; www.springerlink.com
E-mail: jzus@zju.edu.cn

Modelling of flood risks to people and property in a flood diversion zone*

Jun-qiang XIA†1, Peng GUO[1], Mei-rong ZHOU[1], Roger A. FALCONER[2], Zeng-hui WANG[1], Qian CHEN[1]

[1]*State Key Laboratory of Water Resources and Hydropower Engineering Science, Wuhan University, Wuhan 430072, China*

[2]*Hydro-environmental Research Centre, School of Engineering, Cardiff University, Cardiff CF24 3AA, UK*

†E-mail: xiajq@whu.edu.cn

Received Mar. 14, 2018; Revision accepted Aug. 6, 2018; Crosschecked Oct. 18, 2018

Abstract: Extreme floods often occur in the middle Yangtze River. The Jingjiang flood diversion zone needs to be operated during these events to protect the safety of the levees along the Jingjiang Reach. Therefore, it is important to be able to predict the potential flood risks to people and property in such an area for the purpose of flood management. In this study, an integrated numerical model for estimating the flood risks in a flood diversion zone is proposed, including a module for predicting the 2D hydrodynamic processes of flood inundation in a study area with complex topography, and a special module for estimating the flood risks to people (children and adults) and property (vehicles, buildings, and crops) using newly developed safety criteria. The proposed model was used to predict the flood inundation process and variation in hazard degrees of people and property, based on a hypothetical discharge hydrograph during the operation of the Jingjiang flood diversion zone. The model predictions show high flood loss rates for various flooded objects such as people, vehicles, buildings, and crops, with a mean loss rate for these subjects of 75% after 140 h. This suggests that the operation of a flood diversion zone should be cautiously considered, as it would likely result in a huge loss of people and property. Furthermore, an investigation was conducted into the effects of different roughness coefficients and people stability criteria on the model predictions. The results show that variable Manning's roughness coefficients need to be used in the hydrodynamic module according to different underlying surface conditions, and a mechanics-based criterion for the stability of people in floodwaters should be adopted to assess the potential hazard degrees.

Key words: People hazard; Property hazard; Flood risk assessment; Numerical modelling; Jingjiang flood diversion zone
https://doi.org/10.1631/jzus.A1800124 **CLC number:** TV122

1 Introduction

Flood is one of the most frequent and devastating types of disasters over the world. Worldwide statistics indicate that flood loss rates of people and property remain at high levels, and it is estimated that economic loss caused by flood disasters accounts for 40% of the total loss from natural disasters (Zou et al., 2013). Therefore, it is essential to be able to predict the potential flood risks to people and property in a flood-prone area such as a flood diversion zone.

Inundation processes in flood-prone areas are often simulated by 2D hydrodynamic models (Hunter et al., 2008; Neal et al., 2009; Song et al., 2011; Zou et al., 2013; Liu et al., 2015). For example, a raster-based 2D model (Bates and de Roo, 2000) was used to simulate the floodplain inundation process along a 16 km reach of the river Severn in central England. The dynamic performance of the model was validated using airborne synthetic aperture radar images (Bates et al., 2006). Flood risk maps obtained using these numerical models usually present the distributions of

* Project supported by the National Natural Science Foundation of China (Nos. 51725902 and 51579186), the Key Cultivating Project from Wuhan University (No. 2042017kf0238), the Global Challenges Research Fund at Cardiff University, and the UK-China Urban Flooding Research Impact Programme

ORCID: Jun-qiang XIA, https://orcid.org/0000-0001-7613-3457

maximum water depths and velocities for different flood events, but cannot account for the instability mechanisms of people and vehicles in floodwaters (Ni and Xue, 2003; Zou et al., 2013; Alfieri et al., 2014; Metcalfe et al., 2017). For example, Zou et al. (2013) proposed a new model to give a comprehensive flood risk assessment based on the fuzzy analytic hierarchy process (AHP). The model was used to calculate the flood risks in the Jingjiang flood diversion zone, China. A life safety model (LSM) proposed by BC Hydro, Canada provides the capability to produce a comprehensive range of simulations of possible dam failure scenarios, and the present default version of the LSM accepts the product of depth and velocity as the criterion for people stability (Johnstone et al., 2005). di Mauro and Lumbroso (2008) used the LSM to conduct hydrodynamic studies and modelling of life loss for the 1953 Canvey Island flood in the Thames estuary, UK. However, the estimation of the risk to each flooded object in the model was based on empirical relations or formulas. Therefore, there is an opportunity to improve flood risk assessment in a flood-prone area by integrating a module for estimating hazard degrees (HDs) for people and property based on mechanics-based criteria with a hydrodynamic module.

In this study, we propose an integrated model for predicting the flood risks to people and property in a flood diversion zone. The model includes modules for simulating 2D hydrodynamic processes in flood-prone areas and for estimating the flood risks to people and property (such as vehicles, buildings, and crops). The hydrodynamic module was verified using measurements from a physical model of the Toce River. The integrated model was applied to predict the potential flood risks in the Jingjiang flood diversion zone based on a hypothetical event of flood diversion, with various model-predictions being presented. In addition, we also investigated the effects on the model predictions of different Manning's roughness coefficients and criteria for people stability in floodwaters.

2 An integrated numerical model for flood risk assessment

This section presents an existing 2D hydrodynamic module, a module for assessing flood risks to people and property, and a method for quantifying flood HDs. Together, these comprise an integrated numerical model capable of predicting the flood risks to people and property in a flood diversion zone (Xia et al., 2011a, 2011b).

2.1 Module for 2D hydrodynamics

A set of shallow water equations (SWEs) for 2D flows over a horizontal plane can be used to describe flood inundation in flood-prone areas. The depth-averaged 2D SWEs can be written in a general form as

$$\frac{\partial \boldsymbol{U}}{\partial t}+\frac{\partial \boldsymbol{E}}{\partial x}+\frac{\partial \boldsymbol{G}}{\partial y}=\frac{\partial \tilde{\boldsymbol{E}}}{\partial x}+\frac{\partial \tilde{\boldsymbol{G}}}{\partial y}+\boldsymbol{S}, \tag{1}$$

where $\boldsymbol{U}$ is a vector of conserved variables, $\boldsymbol{E}$ and $\boldsymbol{G}$ are convective flux vectors of flow in the x and y directions, respectively, $\tilde{\boldsymbol{E}}$ and $\tilde{\boldsymbol{G}}$ are diffusive vectors related to the turbulent stresses in the x and y directions, respectively, and $\boldsymbol{S}$ is a source term including bed friction and bed slope. The above terms can be written in detail as:

$$\boldsymbol{U}=\begin{bmatrix} h \\ hu \\ hv \end{bmatrix},\quad \boldsymbol{E}=\begin{bmatrix} hu \\ hu^2+gh^2/2 \\ huv \end{bmatrix},\quad \boldsymbol{G}=\begin{bmatrix} hv \\ huv \\ hv^2+gh^2/2 \end{bmatrix},$$
$$\tilde{\boldsymbol{E}}=\begin{bmatrix} 0 \\ \tau_{xx} \\ \tau_{yx} \end{bmatrix},\quad \tilde{\boldsymbol{G}}=\begin{bmatrix} 0 \\ \tau_{xy} \\ \tau_{yy} \end{bmatrix},\quad \boldsymbol{S}=\begin{bmatrix} 0 \\ gh(S_{\mathrm{bx}}-S_{\mathrm{fx}}) \\ gh(S_{\mathrm{by}}-S_{\mathrm{fy}}) \end{bmatrix}, \tag{2}$$

where u and v are depth-averaged velocities in the x and y directions, respectively; h is the water depth; g is the gravitational acceleration; S_{bx} and S_{by} are the bed slopes in the x and y directions, respectively; S_{fx} and S_{fy} are the friction slopes in the x and y directions, respectively; τ_{xx}, τ_{xy}, τ_{yx}, and τ_{yy} are the components of the turbulent shear stress over the plane. In this module, a simple turbulence mode is used to calculate the turbulent viscosity coefficient, and it is not applicable for simulating the complex separation and reattachment flows in local regions (Xia et al., 2010).

The hydrodynamic module adopts a finite volume method (FVM) to solve the governing equations based on an unstructured triangular mesh, which can

be used in various study domains with complex geometry. At an interface between two neighbouring cells, the flow fluxes can be obtained by an approximate Riemann solver. In the current module, a Roe's approximate Riemann solver with the scheme of monotone upstream scheme for conservation laws (MUSCL) is used to evaluate the normal fluxes across the cell interface. A procedure of predictor-corrector time stepping is used to provide the second-order accuracy in both time and space. Furthermore, a refined procedure for treating wetting and drying fronts is used, which is based on an algorithm developed for a regular grid finite difference model (Xia et al., 2010). This hydrodynamic module was validated using existing analytical solutions to simplified dam-break flow problems and observed data from laboratory and field dam-failure flood events (Xia et al., 2010, 2011a, 2011b). Details of the validation process are omitted here. However, this module has been verified again using the measurements from a physical model of the Toce River.

2.2 Module for estimating flood risks to people and property

In this section, the module for estimating flood risks to people and property is outlined briefly. The methods adopted for the flood risks to people and vehicles were based on mechanics-based equilibrium equations (Xia et al., 2014a, 2014b), and the method used for the flood risk to buildings (EA, 2006) was an indicative assessment taken from an average of damage scale for various building types proposed by Kelman (2002). Flood loss rates for rice and cotton were based on previous studies (Liu et al., 1999; Mei and Ji, 2000).

2.2.1 Estimation of flood risk to people

The HD for a human subject during a flood event varies both in time and place across a flood-prone area, and also depends on the body shape and weight of the subject. In flood risk management, the stability of the human body can be used as a quantitative indicator of the HD of people in floodwaters. The assessment of human body stability usually adopts two different types of criteria (Cox et al., 2010). The first type consists of regressed relations based on laboratory data, using experiments involving real human subjects (Abt et al., 1989; Karvonen et al., 2000), and the second type comprises empirical or theoretical formulae derived from a mechanics-based analysis in which the shape of a human body is simplified as a circular or square cylinder (Jonkman and Penning-Rowsell, 2008; Xia et al., 2014b; Milanesi et al., 2015; Martínez-Gomariz et al., 2016; Conesa-García et al., 2017). In this study, a more mechanics-based formula proposed by Xia et al. (2014b) was used to estimate the stability of people in floodwaters. The formula of critical velocity (U_c) was derived based on the instability mechanism for toppling, given by

$$U_c = \alpha\left(\frac{h_f}{h_p}\right)^{\beta} \times \sqrt{\frac{m_p}{\rho_f h_f^2} - \left(\frac{a_1}{h_p^2} + \frac{b_1}{h_f h_p}\right)(a_2 m_p + b_2)}, \tag{3}$$

where ρ_f is the density of water; h_f is the incoming water depth, usually equaling the water depth at a cell; h_p and m_p are the height the mass of a human body, respectively; α and β are parameters that can be evaluated from experimental data; a_1 and b_1 are non-dimensional coefficients related to the buoyancy force of a human body, with a_1=0.633 and b_1=0.367 for a typical body of a Chinese person; a_2 and b_2 are coefficients determined from the average attributes of a human body, with $a_2=1.015\times10^{-3}$ m^3/kg and $b_2=-4.927\times10^{-3}$ m^3. Eq. (3) accounts for the force exerted on the flooded human body due to the body buoyancy and the effect of flood flows with non-uniform velocity distribution along the vertical direction.

A total of 46 tests were conducted in a laboratory flume to investigate the conditions of depth and velocity at toppling instability for a model human body. The best fit between the calculated and measured critical velocities was obtained with the calibrated parameters of α=3.472 m$^{0.5}$/s and β=0.188 (Xia et al., 2014b). The toppling stability thresholds for children and adults were calculated using Eq. (3). Fig. 1a shows the relationships between the water depth and the corresponding incipient velocities for a typical 7-year-old child with a height of 1.26 m and a mass of 25.5 kg, and for an adult with a height of 1.71 m and a mass of 68.7 kg. The incipient velocity for an adult under an incoming depth of 0.5 m is 1.3 m/s, much greater than the velocity for a child (0.8 m/s). As commented by Milanesi et al. (2015), Eq. (3)

represents the state of the art in this field. However, this formula needs to be validated further using more field measurements in urban flood events (Chanson and Brown, 2015).

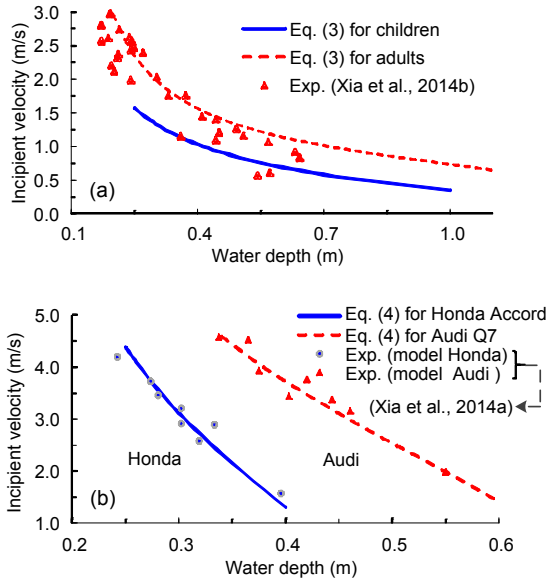

Fig. 1 Stability thresholds in floodwaters for people (a) and vehicles (b) (exp. means experiment)

2.2.2 Estimation of flood risk to vehicles

Different criteria of vehicle stability in floodwaters have been proposed in the form of incipient velocity (Shand et al., 2011), most of which are based on experimental studies and analytical results (Keller and Mitsch, 1993; Xia et al., 2014a; Martínez-Gomariz et al., 2017). Recent studies on flood hazards have shown that vehicles in urban or floodplain areas are generally swept away under various flow conditions. Mechanics-based analysis of a partially-submerged vehicle parking on a flooded street often involves four forces: the drag force, the effective weight, the normal reaction force from the ground, and the frictional force between the tyres and the ground surface. The wheels of a vehicle are assumed to be locked against any rolling movement as it parks on a street, thus a frictional force is produced to resist the vehicle from sliding on the ground surface. According to the theory of sliding equilibrium, a formula of incipient velocity was then derived for commonly used vehicles subject to floodwaters (Xia et al., 2014a). This formula is written as

$$U_c = \alpha\left(\frac{h_f}{h_c}\right)^{\beta} \times \sqrt{2gl_c\left(\frac{\rho_c h_c}{\rho_f h_f} - R_f\right)}, \tag{4}$$

where ρ_c is the density of a vehicle. The vehicle dimensions are characterized by the length l_c, width b_c, and roof height h_c. $R_f=h_c\rho_c/(\rho_f h_k)$, where h_k is the critical water depth at which the vehicle starts to float. Both α and β are parameters related to vehicle shape, tyre type, and roughness of road surface, which need to be determined by laboratory experiments.

Two model vehicles including a Honda Accord (i.e. a small passenger vehicle) and an Audi Q7 (a 4-wheel drive saloon vehicle) were used to conduct the threshold experiments of vehicle instability in a laboratory flume. Based on the experimental data, α=0.212 and β=−0.562 were calibrated for the Honda vehicle, and α=0.438 and β=−0.367 for the Audi vehicle (Xia et al., 2014a). The stability thresholds for these vehicles were calculated using Eq. (4), and Fig. 1b shows the relationship between the water depth and the incipient velocity for these two vehicles. The incipient velocity for the Honda vehicle under a water depth of 0.4 m is 1.3 m/s, which is less than the incipient velocity for the Audi vehicle (3.7 m/s). However, these coefficients in Eq. (4) may need to be adjusted slightly owing to different tyre types and degrees of roughness of the road surface, and should be used carefully in making practical predictions.

2.2.3 Estimation of flood risk to buildings

Forces acting on buildings in floodwaters include mainly hydrostatic, hydrodynamic, and erosion actions, and each category may contain several specific forms of actions (Kelman and Spence, 2004). However, a hierarchy analysis indicates that the main factor in most flood events is the difference between water levels outside and inside a building and the velocity near the building walls. A simplified assessment matrix for the flood risk to buildings proposed by Environment Agency (EA, 2006) was adopted in this study. This matrix represents an average of HD pertaining to various building types in each combination of depth difference and velocity, which can also be approximated by a simple regression relation (Xia et al., 2011a):

$$\mathrm{HD} = 0.7U^{0.14}\Delta h^{0.34}, \tag{5}$$

where U is the velocity near the building, $U=(u^2+v^2)^{1/2}$; Δh is the difference between water levels outside and inside a building; HD is the hazard degree or loss rate of a building in floodwaters. In the initial evaluation, it is difficult to calculate accurately the value of Δh without the detailed structure and layout of a building, and it is assumed that Δh is approximately equal to half the depth at a computational cell. Eq. (5) shows that the HD of a building at a specified incoming velocity of 2 m/s can range from 0 to 0.98, as the value of Δh increases from 0 to 2 m. Note that this regression relation provides only an indicative assessment of the damage that will occur to buildings in flood-prone areas, and does not take account of the effect of different types of buildings. An attempt to consider the building types may bring more uncertainty due to the limited prediction accuracy of the flow parameters around a building. In general, Eq. (5) is acceptable for a preliminary estimation of flood risk to buildings in a flood diversion zone.

2.2.4 Estimation of flood risk to crops

The operation of a flood diversion zone inevitably causes a heavy loss of crops, and significant amounts of rice and cotton harvests would be washed away (Zou et al., 2013). Flood loss rates for crops in a flood diversion zone usually depend on the local flow conditions and the corresponding submergence duration (Liu et al., 1999; Mei and Ji, 2000; Dutta et al., 2003). Statistical data indicate that rice and cotton are two important crops cultivated in the Jingjiang flood diversion zone, and their flood loss rates are closely related to the two factors of water depth and submergence duration (Mei and Ji, 2000). A regression analysis was conducted of the statistical data of flood loss rates for different types of crops in various flood-prone areas collected in previous studies (Liu et al., 1999; Mei and Ji, 2000). The flood loss rates for rice and cotton under different depths and submergence durations are presented in Fig. 2. As shown in Fig. 2a, the loss rate of rice at a water depth ranging from 0.5 m to 1.0 m can reach over 60% under a submergence duration of 3.5 d, while it is over 80% for cotton for the same duration.

2.3 Method for quantifying flood hazard degrees

In this integrated numerical model, Eq. (3) proposed by Xia et al. (2014b) is used to evaluate the degree of people safety in floodwaters, and the incipient velocity formula Eq. (4) is adopted to assess the degree of vehicle safety (Xia et al., 2014a). Therefore, the model adopts mechanics-based formulae to determine the safety degrees of people and vehicles in floodwaters. Although it is very difficult to accurately define the HD for people and vehicles, we expect that as the local velocity approaches the critical value, the HD will be equal to 1.0. Thus, the corresponding HD can be quantified with the following dimensionless index:

$$\mathrm{HD}=\min\left(1.0, U/U_{\mathrm{c}}\right), \tag{6}$$

where HD is the hazard degree or potential loss rate for people or vehicles in floodwaters. People or vehicles will be safe if HD=0, which means that the value of U is much less than the value of U_{c}, namely $U\ll U_{\mathrm{c}}$; they will be in danger if HD approaches 1.0, namely $U\geq U_{\mathrm{c}}$. The values calculated using Eq. (5) and in Fig. 2 can be used directly to quantify the loss rates of buildings or crops in floodwaters. However, more detailed algorithms or modules for evacuation and determination of optimal escape routes need to be developed in the future, and the obtained results can be used in the decision-making system for flood management.

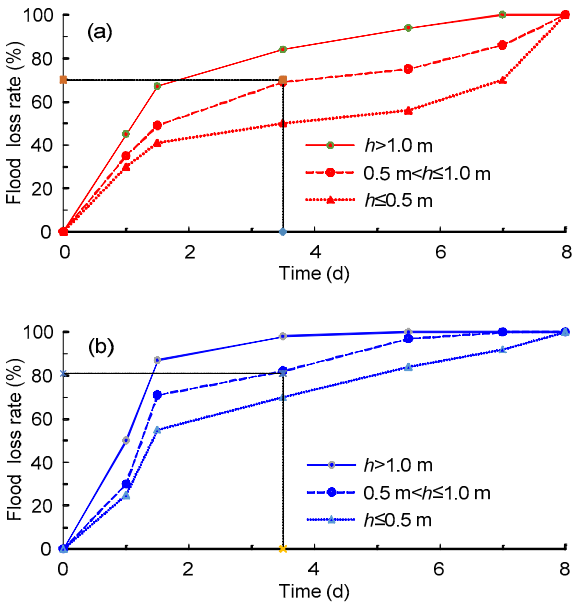

Fig. 2 Flood loss rates at different depths and submergence durations for rice (a) and cotton (b)

2.4 Verification of the hydrodynamic module

To estimate the flood risks to people and property in floodwaters, simulation of flood inundation processes is a key step. Therefore, the 2D hydrodynamic module was verified again using experimental data of flood flows from a physical model of the Toce River. The physical model was built at the ENEL HYDRO laboratories in Milan, Italy, and consisted of a 1:100 scaled replica of almost a 5 km reach of the river.

A large reservoir was located in the central part of the physical model (Fig. 3), and several water probes in the model were used to record the variations in water level at different sites (Soares-Frazao and Testa, 1999). The study domain was divided into 21396 unstructured triangular cells. The minimum and maximum cell areas were 10 cm^2 and 736 cm^2, respectively, with the mesh being locally refined around the upstream, downstream boundaries and the reservoir. The initial bed in the study domain was dry, and the corresponding water depth was set to 0.001 m. The discharge hydrograph at the inflow boundary is shown in Fig. 4. A free outflow boundary condition was applied at the two downstream outlets. A constant time step of Δt=0.001 s and a constant Manning's roughness coefficient of n=0.0162 $m^{-1/3}s$ were used in the hydrodynamic module (Soares-Frazao and Testa, 1999).

Fig. 5 shows comparisons between the calculated and measured water levels at observation points P_1, P_5, P_{10}, and P_{19}. The calculated water depths were generally in close agreement with the measured water depths, with correlation coefficients of R^2=0.84, 0.82, 0.85, and 0.88, respectively. We conclude that the 2D hydrodynamic module can predict the variation in hydrodynamic factors in a flood-prone area with complex topography.

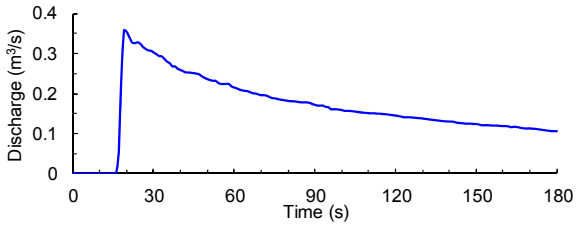

Fig. 4 Discharge hydrograph at the inflow boundary

3 Model application to a flood diversion zone

3.1 Study area

Extreme floods often occur in the Jingjiang Reach of the middle Yangtze River, and the Jingjiang flood diversion zone needs to be operated during these extreme flood events to protect the safety of the levees along the Jingjiang Reach. The flood diversion zone is located on the right side of the Jingjiang Reach, with an effective water storage capacity of 5.4×10^9 m^3 at a level of 42 m (Ni and Xue, 2003). The main engineering of this zone consists of the north sluices for flood diversion, the south sluices for flood release, and closing levees with a total length of 208 km (Fig. 6a). It was first operated in 1954 by successively opening the sluices three times to divert excess flood water. The maximum diversion

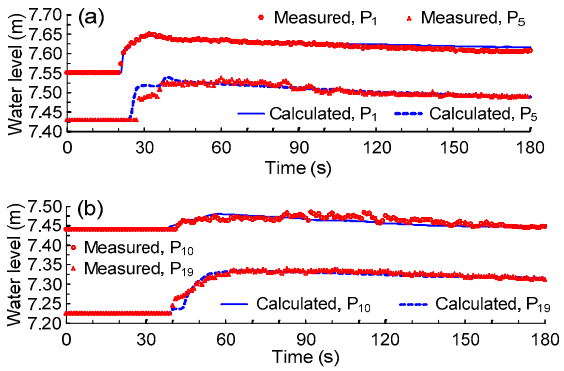

Fig. 5 Comparisons between the calculated and measured water levels at different points: (a) P_1 and P_5; (b) P_{10} and P_{19}

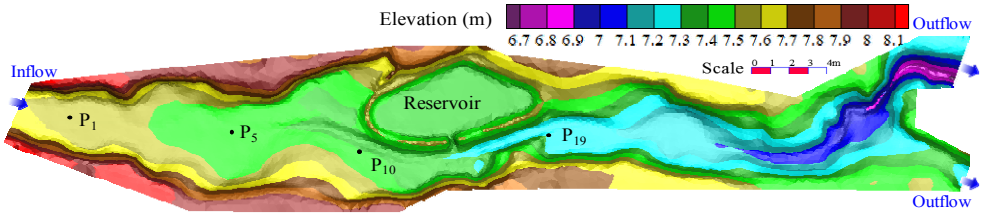

Fig. 3 Topography of a physical model for the Toce River with the locations of four observation points

discharge was 7760 m^3/s, with a total flood diversion volume of 12.26 billion m^3, which reduced the maximum water level at Shashi by 0.96 m. This operation of flood diversion played an important role in ensuring the safety of the levees along the Jingjiang Reach and Wuhan city (Zou et al., 2013).

The flood diversion zone currently covers eight towns and 211 villages, with fixed assets of about 9 billion CNY. The area of towns and villages is 178 km^2, which accounts for about 20% of the total study area. It is estimated that this flood diversion zone has a population of 5.28×10^5 and about 2.0×10^4 vehicles (Zou et al., 2013). The operation probability of the Jingjiang flood diversion zone is estimated to be once in more than 100 years, owing to the operation of the Three Gorges Project. However, this zone is regarded as an important area for flood storage and retention in the flood control systems of the middle Yangtze River. Therefore, it is essential to predict the potential flood risks to people and property in this zone during an extreme flood event.

3.2 Computational conditions

The study area covers the total Jingjiang flood diversion zone, with an area of 921 km^2. In this zone, the length from south to north is 68 km, while the width from east to west is 13.6 km. This flood diversion zone includes various landform units, such as farmland, forest land, villages, and towns (Fig. 6a). The study domain was divided into 11 121 unstructured triangular cells, and the mesh around the sluice gates and near the narrowest site was locally refined, with minimum and maximum cell areas of 3 700 and 420 000 m^2, respectively (Fig. 6b). Fig. 6c shows the bed topography of the study domain, which was interpolated from the limited measured points of bed levels, obtained mainly from the digital elevation database of shuttle radar topography mission (SRTM) 90 m and measured in early 2000. Variable Manning's roughness coefficients were set according to different underlying surface conditions, with values for farmland, forest land, lake area, and village or town of 0.055, 0.065, 0.025, and 0.100 $m^{-1/3}s$, respectively. In addition, the minimum water depth for treating the wetting and drying fronts was set to 0.005 m. The location of the north sluices in the domain was set as an inflow boundary for the flood diversion zone. An assumed discharge hydrograph was used at this inflow boundary (Fig. 7), which was similar to the first hydrograph of the 1954 flood diversion process.

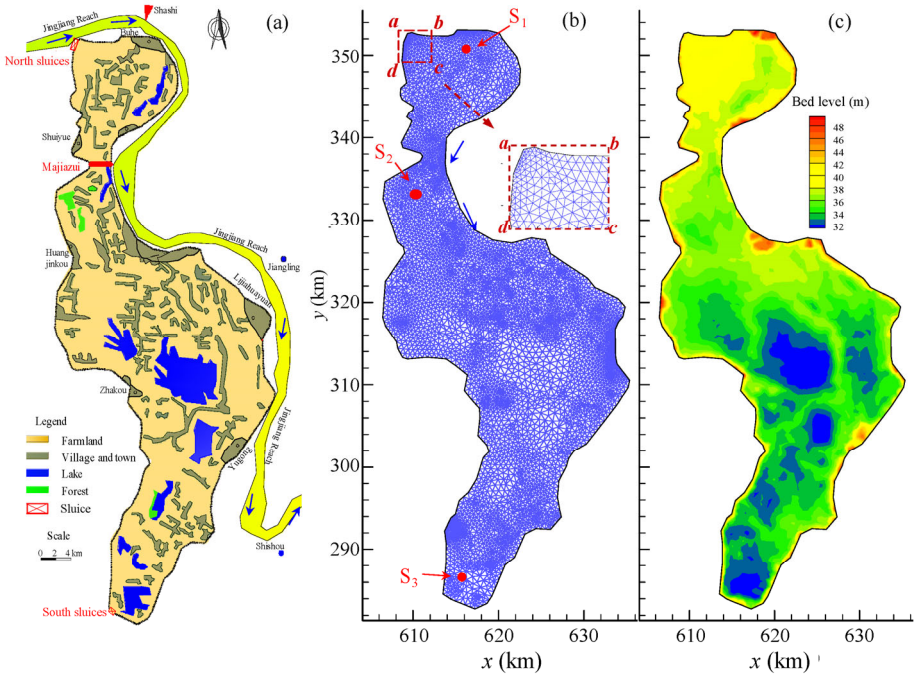

Fig. 6 Jingjiang flood diversion zone: (a) sketch map; (b) computational mesh; (c) bed topography

This flood diversion process lasted for 140 h, with a peak discharge of 6610 m^3/s and an average diversion discharge of 4970 m^3/s (Fig. 7). We assume that the south sluices for flood release would not be operated over this period. The computer time for each simulation scenario was about 35 min in this case.

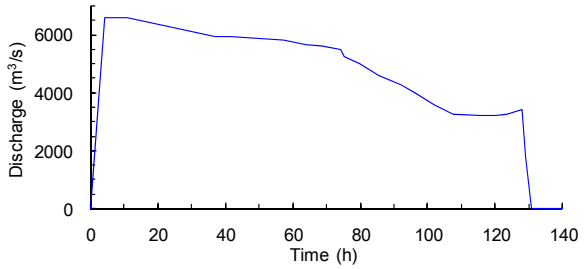

Fig. 7 Discharge hydrograph at the north sluices

3.3 Predicted distributions of depth and velocity at different times

Figs. 8a and 8b indicate the distributions of depth and velocity in the flood diversion zone at different times. After 12 h, with the operation of the north sluices, the flood wave would propagate near the narrowest site of Majiazui in the flood diversion zone, with the maximum depth reaching over 4 m, and with the zone of maximum velocities locating near the sluice gates (Fig. 8a). At t=60 h, the diverted flood water would move to Yugong town, and the majority of the area north of Yugong town would be inundated fully, with water depths in four areas of land or lake approaching 4 m (Fig. 8b). The total flood diversion zone would be submerged at t=90 h, with the maximum depth reaching 6 m. Therefore, such an extreme flood event would lead to a severe loss of human life and property due to the occurrence of both large depths and high velocities.

3.4 Predicted flood risks to people and property

To investigate the temporal variations in the flood risks to people and property at specific sites, three observation sites (S_1, S_2, and S_3) were setup in the flood diversion zone, located respectively near the towns of Buhe and Huangjinkou, and near the south sluices (Figs. 6a and 6b). The water depth at S_1 would reach 1.80 m at t=17 h, with a corresponding flow velocity of 0.34 m/s, which could cause a significant hazard to any human subjects or vehicles (Fig. 9a). However, the loss rate would be lower for crops or buildings. As mentioned above, the loss rate for a specific crop is proportional to the duration of submergence. The degree of damage to buildings in

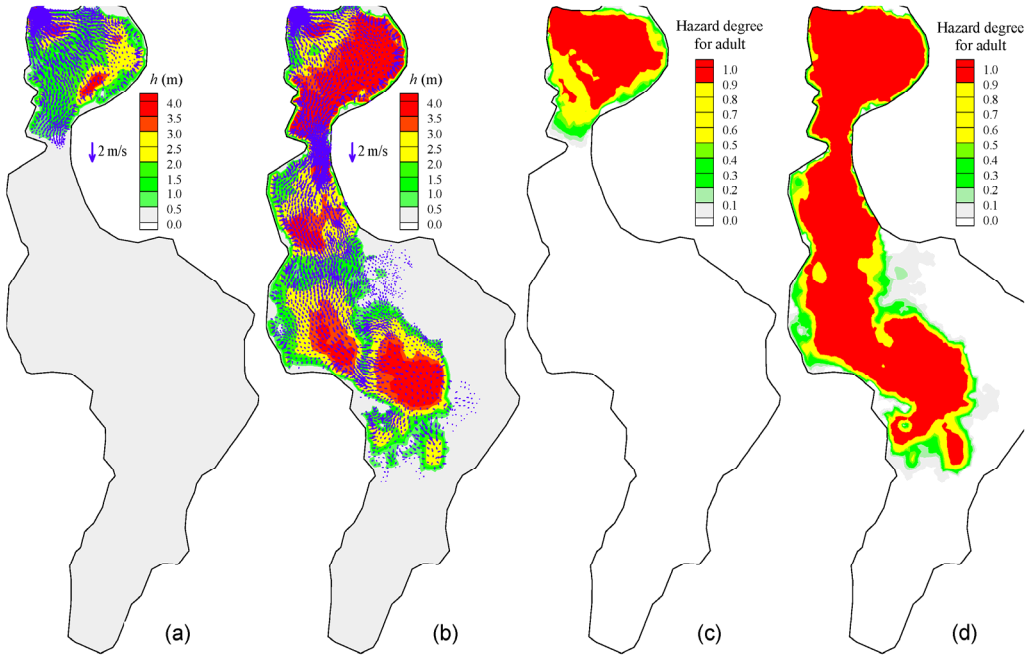

Fig. 8 Distributions of depth and velocity at times t=12 h (a) and t=60 h (b) and flood hazard degree for adults at times t=12 h (c) and t=60 h (d)

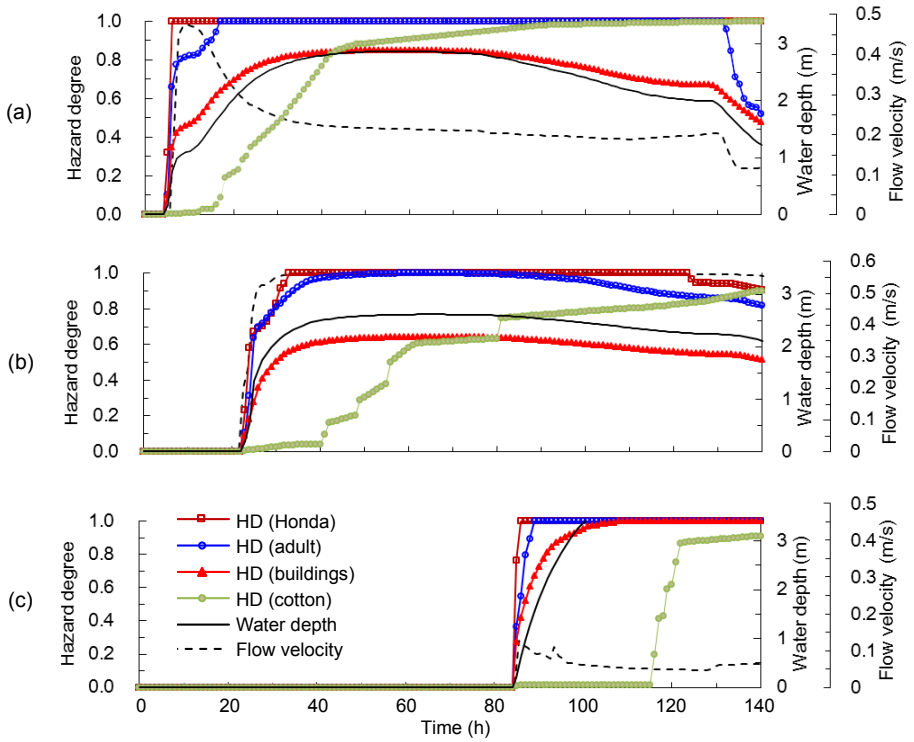

Fig. 9 Temporal variations in flood hazard degrees for adults, vehicles, buildings, and crops at different sites: (a) S_1; (b) S_2; (c) S_3

floodwaters is associated mainly with the local hydrodynamic factors such as depth and velocity, and tends towards a certain value under the given hydrodynamic conditions. The local region around the site of S_2 would start to be inundated at t=22 h, and the HDs of people and property would then increase gradually owing to an increase in water depth and flow velocity (Fig. 9b). Therefore, we conclude from these results that the process of flood inundation due to the operation of the diversion zone would cause serious damage to both people and property because of large water depths and high velocities. Spatial distributions of flood risk to people at different times are shown in Figs. 8c and 8d. At t=12 h, the people in the majority of the area north of Majiazui could be in danger since the values of HD were predicted to approach 1.0 (Fig. 8c). However, it was predicted that at t=60 h, most of the inundated area in the study domain would be dangerous to the local inhabitants due to higher water depths (Fig. 8d).

To estimate the average flood loss rate for each flooded object at a given time, the following calculation method was adopted. The flood loss rate at each computational cell for a specified flooded object (ΔL_i) was calculated using Eq. (5), Eq. (6), or the curves in Fig. 2, with the product of the loss rate at a cell and the corresponding submerged area (ΔA_i) being obtained. The average flood loss rate in the study domain for the given flooded object (ΔL) was defined as the ratio of the summation of this product at the cells to the corresponding total area in which the flooded object is present, which can be written as $\Delta L = \sum_i^{N_k} (\Delta L_i \Delta A_i) \Big/ \sum_i^{N_k} \Delta A_i$, where N_k is the number of computational cells in which a specified flooded subject is present. Note that one computational cell with a specified landform unit can have different flooded subjects. For example, the flood risks to people, vehicles, and buildings need to be considered at the same time at the cells with the attribute of villages and towns. Fig. 10 shows the temporal variations in average flood loss rates for adults, vehicles, buildings, and crops (rice and cotton). With flood inundation in the domain, the average flood loss rate for each object would increase gradually. The flood loss rate at t=140 h could reach 84% for adults and 81% for vehicles (Honda), while it would be 60% for buildings in villages and towns. The variation in the flood loss rate for cotton would differ slightly from that for rice, and the final flood loss rate for rice or

cotton would reach over 60%. Therefore, these model-predictions indicate that the operation of a flood diversion zone should be considered cautiously, because once operated it will usually result in a huge loss of people and property.

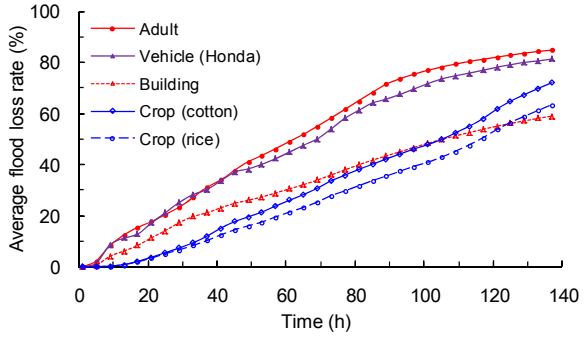

Fig. 10 Temporal variations in average flood loss rates for adults, vehicles, buildings, and crops

There are two additional issues that need to be addressed in future studies. In terms of the flood risk to people, mortality is defined as the ratio of the number of fatalities to the number of people exposed to floodwaters. Jonkman et al. (2008) analyzed empirical information from historical floods, and proposed new mortality functions related to flood characteristics such as depth and velocity. Because the detailed spatial distribution of the population was not available, the mortality of people in floodwaters was not considered in the current study. This needs to be coupled with the current model in the future. Previous studies usually focused on modelling of hydrodynamic processes in this diversion zone (Wang et al., 1998; Cheung and Shao, 2010; Song et al., 2011; Liu et al., 2015). To predict the potential flood risks to people and property in a future flood event, more data need to be collected in advance, covering the discharge hydrograph released from the Three Gorges Reservoir, the detailed regulation mode of the diversion zone, and accurate topography.

4 Discussion

Two issues were considered in this study: the effects on model predictions of different roughness coefficients and of criteria for assessing the stability of people. The first issue was addressed by adopting variable and constant Manning's roughness coefficients in the study domain to investigate their influence on the flood inundation process. The results may provide a basis for further flood risk assessment. The second issue was addressed by comparing the flood HDs based on two kinds of people stability criteria. A detailed investigation of these two issues is presented as follows.

4.1 Effect of different roughness coefficients

Manning's roughness coefficient is an important parameter in the hydrodynamic module, as it can influence the temporal and spatial variations in water depth and flow velocity. A constant Manning's roughness coefficient is often adopted in previous models, but it is not suitable for flood diversion zones, because they contain a variety of landform units which may greatly affect the process of flood inundation. Therefore, in this study variable Manning's roughness coefficients were set according to different underlying surface conditions, and different roughness coefficients were used for various landform units, as mentioned in the above calculation.

To investigate the effect of Manning's roughness coefficients, coefficients ranging from 0.040 to 0.060 $m^{-1/3}s$ for all the underlying surfaces were adopted to simulate the flood inundation process in the Jingjiang flood diversion zone. The locations of the three observed sites (S_1, S_2, and S_3) are shown in Fig. 6b, and the corresponding temporal variations in water depth and flow velocity under different Manning coefficients are presented in Figs. 11 and 12. The results show that the maximum water depth would increase and the corresponding maximum flow velocity would decrease with an increase in Manning's roughness coefficient at sites S_1 and S_2. At these sites located close to the diversion sluices, the flood arrival times were almost the same under different scenarios, and the model predictions using a unified Manning's roughness coefficient of n=0.060 $m^{-1/3}s$ were in close agreement with the results using the variable Manning's roughness coefficients.

However, at site S_3 located near the south sluices, the temporal variations in water depth under these scenarios were obviously different, with flood arrival times ranging from 72 to 88 h (Fig. 11c), and maximum flow velocities of 0.18, 0.17, 0.15, and 0.13 m/s (Fig. 12c). Therefore, we conclude that different

Manning's roughness coefficients can greatly influence the flood propagation process, and have an important impact on the associated flood risk assessment.

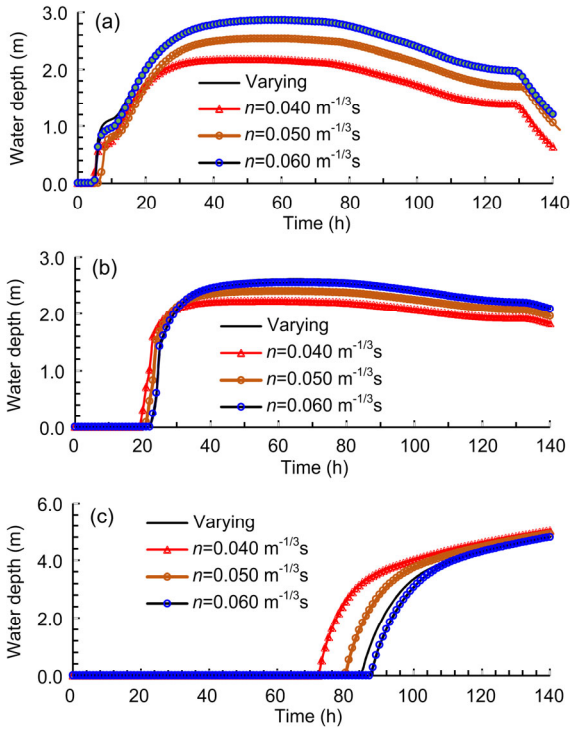

Fig. 11 Temporal variations in water depth under different Manning's roughness coefficients at different sites: (a) S_1; (b) S_2; (c) S_3

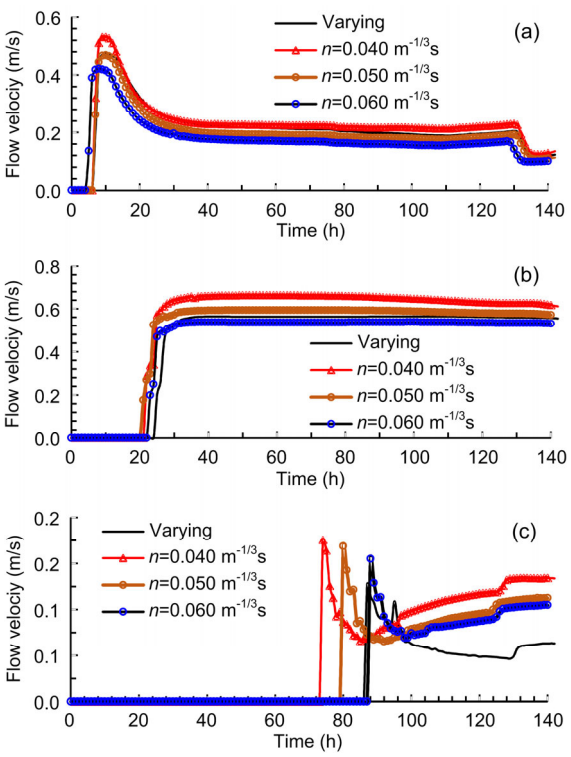

Fig. 12 Temporal variations in flow velocity under different Manning's roughness coefficients at different sites: (a) S_1; (b) S_2; (c) S_3

4.2 Effect of criteria for people stability

Various criteria for people stability in floodwaters have been proposed recently for flood risk management. For example, Cox et al. (2010) proposed hazard regimes as a function of depth and velocity based on available experimental data. There are four hazard levels: low hazard ($0 \le h \times U < 0.6$) (m^2/s), moderate hazard ($0.6 \le h \times U < 0.8$), significant hazard ($0.8 \le h \times U < 1.2$), and extreme hazard ($h \times U \ge 1.2$, $h \ge 1.2$, or $U \ge 3.0$). The HD for people was calculated by $(h \times U)/1.2$. People are considered to be in danger if the HD approaches 1.0, namely $h \times U \ge 1.2$, $h \ge 1.2$, or $U \ge 3.0$.

Comparisons between the calculated HDs of people at sites S_1, S_2, and S_3 are shown in Fig. 13. HD was estimated using two kinds of stability criteria in floodwaters as proposed by Cox et al. (2010) and Xia et al. (2014b). We found that there was a continuous change in HD at each observation site using the criterion of Xia et al. (2014b) and a discontinuous change in HD at t=11, 25, and 87 h at sites S_1, S_2, and S_3, respectively, using the criterion of Cox et al. (2010). Hydrodynamic factors and HDs at these sites at characteristic times are also presented in Table 1. For example, the flood factors at S_1 were almost the same at t=11 and 12 h, but the values of HD calculated using the criterion of Cox et al. (2010) were different because of the critical water depth of 1.20 m. At S_2 at t=24 h and at S_3 at t=87 h, flow velocities were less than 0.30 m/s, leading to small values of HD calculated using the criterion of Cox et al. (2010). We conclude that the HD of people in floodwaters calculated using the criterion of Cox et al. (2010) greatly depends on the velocity if the water depth is less than the critical value of 1.20 m, but their criterion cannot account for the effect of velocity if the water depth exceeds 1.20 m. Therefore, the mechanics-based criterion of people stability in floodwaters proposed by Xia et al. (2014b) would be more reliable and effective in estimating HDs because the effects of both

water depth and flow velocity are considered in the criterion.

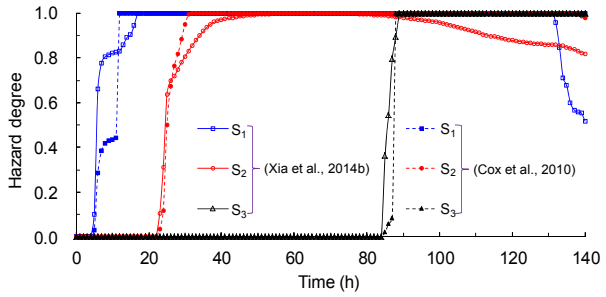

Fig. 13 Comparisons of hazard degrees of people in floodwaters at sites S_1, S_2, and S_3 using two kinds of stability criteria

Table 1 Comparisons of hazard degrees estimated by two kinds of stability criteria at sites S_1, S_2, and S_3

Site	Time (h)	h (m)	U (m/s)	$h\times U$ (m^2/s)	HD (Cox et al., 2010)	HD (Xia et al., 2014b)
S_1	11	1.16	0.46	0.53	0.44	0.83
	12	1.21	0.44	0.54	1.00	0.83
	17	1.74	0.34	0.59	1.00	1.00
S_2	24	0.55	0.26	0.14	0.12	0.41
	25	1.36	0.44	0.60	1.00	0.85
	26	1.58	0.51	0.81	1.00	0.97
	27	1.74	0.53	0.92	1.00	1.00
S_3	87	0.95	0.11	0.10	0.08	0.60
	88	1.27	0.09	0.12	1.00	0.75
	89	1.54	0.09	0.14	1.00	1.00
	90	1.79	0.09	0.17	1.00	1.00

5 Conclusions

1. An integrated numerical model for estimating the flood risks to people and property in a flood diversion zone is proposed, including a module for predicting the 2D hydrodynamic processes in a flood-prone zone with complex topography, and a special module for predicting the flood risks to people and property using mechanics-based and empirical formulae.

2. The flood inundation processes and the variation in the HDs of people and property were predicted for a hypothetical process of flood diversion using the proposed model. The predicted flood loss rates for adults, vehicles, buildings, and crops were relatively high, with a mean loss rate for these subjects of 75% after 140 h. Therefore, the operation of a flood diversion zone should be considered cautiously in flood risk management.

3. Effects on the model predictions of different roughness coefficients and people stability criteria were investigated. The results show that it is necessary to set up variable Manning's roughness coefficients according to different underlying surface conditions in the hydrodynamic module, because they can influence the temporal and spatial variation in water depth and velocity, and a mechanics-based criterion of people stability in floodwaters should be adopted to assess the potential flood HDs.

References

Abt SR, Wittier RJ, Taylor A, et al., 1989. Human stability in a high flood hazard zone. *Journal of the American Water Resources Association*, 25(4):881-890. https://doi.org/10.1111/j.1752-1688.1989.tb05404.x

Alfieri L, Salamon P, Bianchi A, et al., 2014. Advances in pan-European flood hazard mapping. *Hydrological Processes*, 28(13):4067-4077. https://doi.org/10.1002/hyp.9947

Bates PD, de Roo APJ, 2000. A simple raster-based model for flood inundation simulation. *Journal of Hydrology*, 236(1-2):54-77. https://doi.org/10.1016/S0022-1694(00)00278-X

Bates PD, Wilson MD, Horritt MS, 2006. Reach scale floodplain inundation dynamics observed using airborne synthetic aperture radar imagery: data analysis and modelling. *Journal of Hydrology*, 328(1-2):306-318. https://doi.org/10.1016/j.jhydrol.2005.12.028

Chanson H, Brown R, 2015. New criterion for the stability of a human body in floodwaters. *Journal of Hydraulic Research*, 53(4):540-541. https://doi.org/10.1080/00221686.2015.1054321

Cheung RWK, Shao SD, 2010. Revisiting a flood simulation model based on PIC techniques. *Proceedings of the Institution of Civil Engineers-Engineering and Computational Mechanics*, 163(4):235-242. https://doi.org/10.1680/eacm.2010.163.4.235

Conesa-García C, García-Lorenzo R, Pérez-Cutillas P, 2017. Flood hazards at ford stream crossings on ephemeral channels (south-east coast of Spain). *Hydrological Processes*, 31(3):731-749. https://doi.org/10.1002/hyp.11082

Cox RJ, Shand TD, Blacka MJ, 2010. Australian Rainfall and Runoff Project 10: Appropriate Safety Criteria for People. Technical Report No. P10/S1/006, Water Research Laboratory, Manly Vale, Australia.

di Mauro M, Lumbroso D, 2008. Hydrodynamic and loss of

life modelling for the 1953 Canvey Island flood. Proceedings of the International Conference on Flood Risk, p.1117-1126.

Dutta D, Herath S, Musiake K, 2003. A mathematical model for flood loss estimation. *Journal of Hydrology*, 277(1-2): 24-49. https://doi.org/10.1016/S0022-1694(03)00084-2

EA (Environment Agency), 2006. Flood and Coastal Defence R&D Programme, R&D Outputs: Flood Risks to People (Phase 2). Technical Report No. FD2321/PR, Environment Agency, Department for Environment, Food and Rural Affairs, UK.

Hunter NM, Bates PD, Neelz S, et al., 2008. Benchmarking 2D hydraulic models for urban flooding. *Proceedings of the Institution of Civil Engineers-Water Management*, 161(1): 13-30. https://doi.org/10.1680/wama.2008.161.1.13

Johnstone WM, Sakamoto D, Assaf H, et al., 2005. Architecture, modelling framework and validation of BC hydro's virtual reality life safety model. Proceedings of the 9th International Symposium on Stochastic Hydraulics, p.23-24.

Jonkman SN, Penning-Rowsell E, 2008. Human instability in flood flows. *Journal of the American Water Resources Association*, 44(5):1208-1218. https://doi.org/10.1111/j.1752-1688.2008.00217.x

Jonkman SN, Vrijling JK, Vrouwenvelder ACWM, 2008. Methods for the estimation of loss of life due to floods: a literature review and a proposal for a new method. *Natural Hazards*, 46(3):353-389. https://doi.org/10.1007/s11069-008-9227-5

Karvonen RA, Hepojoki A, Huhta HK, et al., 2000. The Use of Physical Models in Dam-Break Analysis. RESCDAM Final Report, Helsinki University of Technology, Helsinki, Finland.

Keller RJ, Mitsch B, 1993. Safety Aspects of Design Roadways as Floodways. Research Report No. 69, Urban Water Research Association, Melbourne, Australia.

Kelman I, 2002. Physical Flood Vulnerability of Residential Properties in Coastal Eastern England. PhD Thesis, University of Cambridge, Cambridge, UK.

Kelman I, Spence R, 2004. An overview of flood actions on buildings. *Engineering Geology*, 73(3-4):297-309. https://doi.org/10.1016/j.enggeo.2004.01.010

Liu Q, Qin Y, Zhang Y, et al., 2015. A coupled 1D-2D hydrodynamic model for flood simulation in flood detention basin. *Natural Hazards*, 75(2):1303-1325. https://doi.org/10.1007/s11069-014-1373-3

Liu SK, Song YS, Cheng XT, et al., 1999. Flood Risk Assessment and Disaster Mitigation Countermeasures for the Floodplain and Flood Detension Areas in the Lower Yellow River. Yellow River Water Conservancy Press, Zhengzhou, China (in Chinese).

Martínez-Gomariz E, Gómez M, Russo B, 2016. Experimental study of the stability of pedestrians exposed to urban pluvial flooding. *Natural Hazards*, 82(2):1259-1278. https://doi.org/10.1007/s11069-016-2242-z

Martínez-Gomariz E, Gómez M, Russo B, et al., 2017. A new experiments-based methodology to define the stability threshold for any vehicle exposed to flooding. *Urban Water Journal*, 14(9):930-939. https://doi.org/10.1080/1573062X.2017.1301501

Mei YD, Ji CM, 2000. Flood Risk Analysis. Science & Tecnology Press, Wuhan, China (in Chinese).

Metcalfe P, Beven K, Hankin B, et al., 2017. A modelling framework for evaluation of the hydrological impacts of nature-based approaches to flood risk management, with application to in-channel interventions across a 29-km^2 scale catchment in the United Kingdom. *Hydrological Processes*, 31(9):1734-1748. https://doi.org/10.1002/hyp.11140

Milanesi L, Pilotti M, Ranzi R, 2015. A conceptual model of people's vulnerability to floods. *Water Resources Research*, 51(1):182-197. https://doi.org/10.1002/2014WR016172

Neal J, Fewtrell T, Trigg M, 2009. Parallelisation of storage cell flood models using OpenMP. *Environmental Modelling & Software*, 24(7):872-877. https://doi.org/10.1016/j.envsoft.2008.12.004

Ni JR, Xue A, 2003. Application of artificial neural network to the rapid feedback of potential ecological risk in flood diversion zone. *Engineering Applications of Artificial Intelligence*, 16(2):105-119. https://doi.org/10.1016/S0952-1976(03)00059-9

Shand TD, Cox RJ, Blacka MJ, et al., 2011. Australian Rainfall and Runoff Project 10: Appropriate Safety Criteria for Vehicles-Literature Review (Stage 2). Technical Report No. P10/S2/020, Water Research Laboratory, Manly Vale, Australia.

Soares-Frazao S, Testa G, 1999. The Toce River test case: numerical results analysis. Proceedings of the 3rd CADAM Workshop.

Song LX, Zhou JZ, Li QQ, et al., 2011. An unstructured finite volume model for dam-break floods with wet/dry fronts over complex topography. *International Journal for Numerical Methods in Fluids*, 67(8):960-980. https://doi.org/10.1002/fld.2397

Wang GQ, Shao SD, Fei XJ, 1998. Particle model for simulating flow over large areas. *Journal of Hydraulic Engineering*, 124(5):554-557. https://doi.org/10.1061/(asce)0733-9429(1998)124:5(554)

Xia JQ, Falconer RA, Lin BL, et al., 2010. Modelling flood routing on initially dry beds with the refined treatment of wetting and drying. *International Journal of River Basin Management*, 8(3-4):225-243. https://doi.org/10.1080/15715124.2010.502121

Xia JQ, Falconer RA, Lin BL, et al., 2011a. Modelling flash flood risk in urban areas. *Proceedings of the Institution of Civil Engineers-Water Management*, 164(6):267-282. https://doi.org/10.1680/wama.2011.164.6.267

Xia JQ, Falconer RA, Lin BL, et al., 2011b. Numerical assessment of flood hazard risk to people and vehicles in

flash floods. *Environmental Modelling & Software*, 26(8): 987-998. https://doi.org/10.1016/j.envsoft.2011.02.017

Xia JQ, Falconer RA, Xiao XW, et al., 2014a. Criterion of vehicle stability in floodwaters based on theoretical and experimental studies. *Natural Hazards*, 70(2):1619-1630. https://doi.org/10.1007/s11069-013-0889-2

Xia JQ, Falconer RA, Wang YJ, et al., 2014b. New criterion for the stability of a human body in floodwaters. *Journal of Hydraulic Research*, 52(1):93-104. https://doi.org/10.1080/00221686.2013.875073

Zou Q, Zhou JZ, Zhou C, et al., 2013. Comprehensive flood risk assessment based on set pair analysis-variable fuzzy sets model and fuzzy AHP. *Stochastic Environmental Research and Risk Assessment*, 27(2):525-546. https://doi.org/10.1007/s00477-012-0598-5

中文概要

题　目： 分洪区群众生命与财产的洪水风险模拟

目　的： 分洪工程的启用具有非常重要的防洪效益，但同时也将严重威胁分洪区群众的生命财产安全。为定量计算洪水中人体（成人与儿童）、车辆、房屋、农作物（水稻和棉花）的洪水风险与洪灾损失，考虑受淹对象的失稳机理，提出分洪区群众生命与财产的洪水风险模拟模型。

创新点： 1. 基于力学过程中的洪水中人体与车辆失稳的计算公式，建立相应洪水风险等级评定的新方法，并提出 4 类受淹对象平均损失率的计算方法；2. 结合二维水动力学模型的计算结果，分析 4 类受淹对象洪水风险的时空变化情况，同时讨论根据不同下垫面类型取不同糙率值以模拟洪水演进过程的必要性，并比较文献中提出的洪水中人体风险等级计算结果的差异。

方　法： 1. 分析现有洪水中人体、车辆、房屋和农作物风险或损失的计算方法，提出相应洪水风险计算关系或计算曲线（公式（3）~（6），图 1 和 2）；2. 参考 1954 年荆江分洪工程北闸第一次的分洪情况，通过计算分洪区 140 h 的洪水演进过程和 4 类受淹对象洪水风险的时空分布（图 8），同时得到 4 类受淹对象平均损失率随时间的变化情况（图 10）；3. 在荆江分洪区洪水演进过程模拟中，讨论根据不同下垫面类型确定相应糙率值的方法与计算区域糙率统一取值 0.04、0.05 或 0.06 的 3 种工况下洪水要素变化的差异（图 11 和 12），并采用文献中提出的洪水中人体风险等级计算方法，比较洪水中人体风险等级变化的异同（图 13）。

结　论： 1. 一旦荆江分洪工程启用，截止至北闸开启 140 h 时，洪水中人体、车辆、房屋、农作物的平均损失率达到 75%以上，即分洪工程的启用将造成重大的生命财产损失；2. 糙率取值方法的不同，导致洪水演进过程不同，进而影响各类受淹对象的洪水风险评估，因此需要根据不同下垫面类型确定相应的糙率值；3. 文献中提出的洪水中人体风险等级计算方法考虑了人体失稳的力学过程，综合考虑了水深和流速的影响，可以更安全可靠地应用于实际洪水中人体的风险等级评价。

关键词： 人体；财产；洪水风险评估；数学模型；荆江分洪区